Article

Not peer-reviewed version

Power Quality Enhancement of Wind-Battery Supplied Standalone Microgrid by Using Super Twisting Sliding Mode Controllers

Sana Sahbani *, Oumnia Licer , Hassane Mahmoudi , Abdennebi Hasnaoui , Mustapha Kchikach

Posted Date: 31 October 2024

doi: 10.20944/preprints202410.2581.v1

Keywords: Wind System; Battery Storage; Power Quality; Microgrid; HIL; Super Twisting Sliding Mode Controllers; HOA

 doi:10.20944/preprints202410.2581.v1

Article

Power Quality Enhancement of Wind-Battery Supplied Standalone Microgrid by Using Super Twisting Sliding Mode Controllers

Sana Sahbani [1,2], Hassan Mahmoudi [2], Abdennebi Hasnaoui [1,2], Mustapha Kchikach [1,2] and Oumnia Licer [1]

[1] CPS2E laboratory, CCSER Team, Electromechanical Department, Higher National School of Mines, Rabat, Morocco
[2] Electronics Power and Control Team, Department of Electrical Engineering, Mohammadia School of Engineers, Mohammed V University, Rabat, Morocco
* Correspondence: sahbani@enim.ac.ma

Abstract: There is a growing interest among researchers in the creation of innovative power supply systems that incorporate a range of generators, with a specific emphasis on renewable energy sources, especially wind energy. Battery-operated independent Microgrids powered by wind energy are increasingly recognized worldwide as a standalone power source for consumers. The power produced by the wind power conversion system depends on the wind speed, which can change quickly and without warning. It is essential to establish a robust energy management system accompanied by a responsive control approach to attain optimal energy balance and guarantee the delivery of high-quality power. In order to facilitate a rapid and efficient reaction to unexpected variations in the power supply system, the control strategy for the inverter and bidirectional DC to DC converter employs super twisting sliding mode controllers. The voltage at the DC link is controlled to maintain energy equilibrium within the standalone Microgrid, while a distinctive control approach for the three-phase inverter guarantees the delivery of high-quality power to AC loads. The proposed control methodologies in this paper employ super twisting sliding mode controllers to achieve rapid and effective responses during rapid changes in the system, whether on the generation or load side. The Hippopotamus optimization method is developed to obtain accurate values of various parameters used in super twisting sliding mode controllers under various operating conditions. The paper emphasizes the diverse outcomes and knowledge acquired through the execution of Hardware-in-the-Loop simulations utilizing the OPAL-RT platform. By employing this cutting-edge technology, researchers successfully tested and validated various hardware components within a simulated environment, facilitating a more efficient and cost-effective approach to analyzing and optimizing system performance. Further, detailed small signal analysis for the proposed methodology is also included in this paper.

Keywords: wind system; battery storage; power quality; microgrid; HIL; super twisting sliding mode controllers; HOA

1. Introduction

The shift towards renewable energy sources is driven by the urgent need to reduce greenhouse gas emissions and tackle the challenges posed by climate change. The utilization of wind energy [1,2] has become increasingly favored, particularly because of its plentiful nature and sustainable characteristics. Scholars are investigating novel methods to utilize wind energy, including the development of offshore wind farms and the enhancement of turbine technology. Renewable energy sources offer a sustainable and environmentally friendly alternative to traditional fossil fuels, which are finite in supply and play a significant role in environmental degradation. The advancement of innovative power supply systems that harness renewable energy sources is essential for moving towards a more sustainable and eco-friendly energy framework. Through their commitment to research and innovation in this domain, researchers are laying the groundwork for a cleaner and more sustainable future for future generations. Therefore, the implementation of SMSs can address

 doi:10.20944/preprints202410.2581.v1

numerous challenges, such as delivering electricity to consumers, minimizing pollution, and ensuring a reliable and stable power supply. These SMSs can utilize wind energy by employing small-scale wind turbines, which produce electricity that is subsequently stored in batteries for later use. This technology proves to be especially beneficial in remote or off-grid locations where conventional power sources might be inconsistent or inaccessible. Wind-battery powered Microgrids present an environmentally friendly and economically viable option for supplying electricity to residences, enterprises, and communities, thereby decreasing reliance on fossil fuels and minimizing carbon emissions [3]. The growing demand for clean energy has contributed to the heightened popularity of SMSs operated by WPCS-BSU, positioning them as a feasible solution for advancing a more sustainable future. This indicates that the quantity of electricity generated by the WPCS can fluctuate significantly based on the wind speed at any particular time. In conditions of strong winds, the system is capable of producing a substantial amount of power; however, during periods of calm winds, the power output may be minimal or nonexistent. The inconsistency inherent in wind power presents difficulties in depending exclusively on it for stable energy generation, as it does not serve as a constant and dependable energy source. To address this challenge, WPCSs are frequently integrated with various renewable energy sources or energy storage systems, such as BSUs, to provide a more reliable and steady power supply [4–6].

The establishment of a robust EMS is essential for numerous reasons. Primarily, it contributes to attaining an ideal balance of energy in the standalone power supply systems. This indicates that the energy consumption and generation within a system are in equilibrium, thereby ensuring efficient energy utilization and minimizing waste. The implementation of an EMS enables organizations to pinpoint areas of energy inefficiency and undertake essential actions to enhance energy utilization. In addition, a well-functioning EMS is crucial for guaranteeing the delivery of high-quality power. Power quality pertains to the attributes of the electricity supply, encompassing voltage stability, frequency control, and the lack of disturbances or interruptions. An adaptive control approach within the EMS can oversee and adjust these parameters, guaranteeing that the power delivered to consumers adheres to the necessary standards. This holds significant importance for industries and critical infrastructure sectors, as any issues related to power quality may result in equipment damage, production losses, or potential safety risks.

Furthermore, an EMS that employs a responsive control methodology allows organizations to proactively adapt to fluctuations in energy demand and supply. This is especially significant in the current evolving energy environment, where the adoption of renewable energy sources and distributed generation is increasingly common. Through the ongoing observation of energy consumption trends and the incorporation of real-time data, organizations are able to modify their energy usage and production as needed. This approach not only enhances energy efficiency but also facilitates improved integration of renewable energy sources, thereby decreasing dependence on fossil fuels and lessening environmental impact. Furthermore, a well-implemented EMS can lead to significant cost reductions. Organizations can reduce their energy consumption and lower their energy expenses by identifying energy inefficiencies and implementing energy-saving strategies. In addition, an adaptive control strategy can enable organizations to engage in demand response programs, permitting them to adjust their energy usage during peak demand periods to receive financial incentives. The potential for substantial cost reductions is particularly notable in energy-intensive sectors and large commercial facilities.

Super twisting sliding mode controllers represent sophisticated control algorithms specifically developed to ensure robust and precise control in dynamic systems. They demonstrate significant efficacy in systems characterized by uncertain or fluctuating parameters, rendering them an optimal selection for power supply systems that experience abrupt variations. Therefore, the integration of STSM controllers enables the control methodology of the inverter and bidirectional DC to DC circuit to swiftly and precisely adapt to fluctuations in the power supply system. These controllers possess the ability to swiftly modify the output voltage and current of the inverter and bidirectional DC to DC converter to align with the specified values, thereby guaranteeing the stability and reliability of the power supply system. The implementation of STSM controllers significantly improves the overall

 doi:10.20944/preprints202410.2581.v1

efficiency of the power supply system. These controllers are engineered to reduce energy losses and enhance the efficiency of both the inverter and the bidirectional DC to DC converter. Through the ongoing observation and modification of control signals, the controllers guarantee that the power conversion process is executed with optimal efficiency, minimizing energy loss and enhancing the overall functionality of the system.

In addition, the integration of super twisting sliding mode controllers improves the system's capacity to manage abrupt variations in load or input parameters. These controllers possess the ability to swiftly adjust to changes in system parameters, enabling the inverter and bidirectional DC to DC converter to sustain stable operation, even in difficult circumstances. This guarantees that the power supply system is capable of effectively addressing abrupt changes in demand or supply, thereby averting any disruptions or failures within the system. The regulation of voltage at the dc-link is achieved by utilizing a combination of energy storage systems, including batteries and super-capacitors, along with power electronic devices such as dc-dc converters and bidirectional inverters. This guarantees that the energy produced by renewable sources, including wind turbines, is effectively stored and distributed to satisfy the requirements of the AC loads in the SMSs. The distinctive control approach of the three-phase inverter utilizes sophisticated algorithms that oversee and modify the output voltage and frequency, ensuring consistent and dependable power supply to the AC loads. This control strategy encompasses various features, including power factor correction, harmonic filtering, and voltage regulation, to guarantee that high-quality power is delivered to sensitive electronic devices and appliances. The integration of a regulated DC-link voltage with sophisticated control mechanisms for the three-phase inverter enables the SMS to function independently and effectively, ensuring the delivery of dependable and high-quality power to its users while optimizing the use of renewable energy resources.

The document emphasizes the diverse outcomes and knowledge acquired through the execution of HIL simulations utilizing the OPAL-RT platform. By employing this cutting-edge technology, researchers successfully tested and validated various hardware components within a simulated environment, facilitating a more efficient and cost-effective approach to analyzing and optimizing system performance. The results outlined in the paper illustrate the efficacy of employing HIL simulations on the OPAL-RT platform across various applications, including power systems and automotive engineering. The paper highlights the advantages of employing this advanced technology to enhance the design and performance of intricate systems.

The paper is organized by providing detailed description in Section-II, and the process to estimate various parameters of STSM controllers by using HOA is given in Section-III. Detailed mathematical modeling and proposed methodology are provided in Sections-IV and V respectively. Section-VI compressed with small signal analysis of the SMG. Various results are examined using HIL configuration in Section-VII. Conclusion and references are placed at the end of the paper.

2. Standalone Microgrid System

The WPCS and BSU play a crucial role in the renewable energy system proposed by SMS. They collaborate to capture and store wind energy for future utilization. To optimize the use of this energy, they are linked to a common DC-link via their individual converters. The WPCS consists of a wind turbine that converts the kinetic energy of the wind into electrical energy. The electrical energy is subsequently transformed from alternating current (AC) to direct current (DC) through a converter, thereby ensuring its compatibility with the DC-link. The DC-link serves as a pivotal connection, enabling the WPCS to convey the energy it generates to the BSU. The BSU is essential to the system as it retains surplus energy produced by the wind turbine. The accumulated energy is employed during periods of low wind or heightened demand. The BSU is linked to the DC-link via a converter, facilitating bidirectional energy transfer between the WPCS and the BSU.

An inverter is linked to the DC-link in order to supply power to AC loads. The inverter transforms the DC power from the DC-link into AC power, making it appropriate for operating a range of electrical appliances and devices. This enables the use of the energy stored in the BSU or the energy produced by the wind turbine to supply power to residential or industrial loads. The

 doi:10.20944/preprints202410.2581.v1

integration of the WPCS, BSU, and inverter with the common DC-link facilitates a smooth and effective energy transfer throughout the system. It guarantees that the energy produced by the wind turbine is efficiently stored and utilized, thereby offering a dependable and sustainable power source for AC loads. This cohesive system facilitates the enhancement of renewable energy resources and plays a significant role in fostering a more environmentally friendly and sustainable future. Consequently, the WPCS and BSU are connected to a common DC-link via their individual converters. The AC loads are subsequently supplied with power by an inverter that is linked to the DC-link, as depicted in Figure 1. Different control blocks are established through the utilization of STSM controllers. Both three-phase and single-phase AC loads are incorporated at PLB.

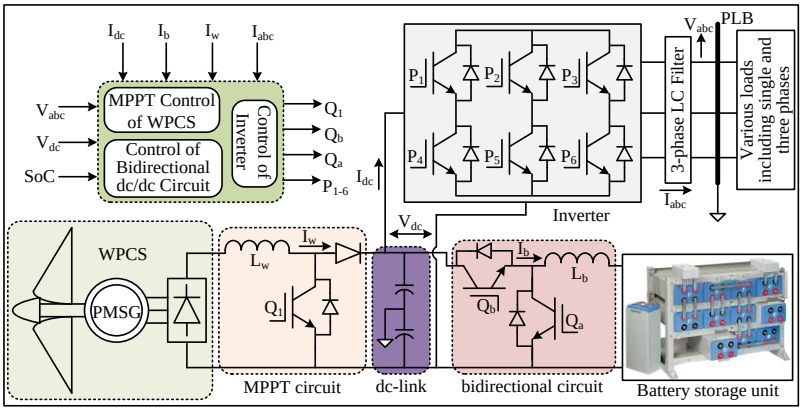

Figure 1. Standalone Microgrid supplied by WPCS-BSU.

A similar type of SMS has been utilized by numerous scholars, and a selection of these examples is presented here. The authors in reference [7] introduced a methodology for controlling voltage and frequency in photovoltaic-based SMS under different variations; however, they did not take into account the WPCS. The authors in [8] have introduced a novel control methodology aimed at enhancing both hydrogen production and power quality in hybrid SMS systems. The authors in references [9,10] introduced a paper aimed at enhancing the power quality of the SMS during fault occurrences in the distribution system through the application of various control strategies. The authors in [11] have presented a methodology for the optimal sizing of the BSU within the WPCS based on SMS. The authors in [12] introduce a grid-integrated hybrid Microgrid system; however, this system is linked to the primary electric grid. Coordinated power management system among various components including wind and battery is developed by authors in [13], however, system is hybrid Microgrid consisting of solar energy, eletrolyzer, fuel cell etc. The authors in [14] introduce frequency load shedding via the droop control strategy utilized in WPCS based SMS. A novel control method is proposed by author in [15] for improving power quality of standalone Microgrid under faults on distribution lines. Authors in [16] presented a hybrid Microgrid supplied by photovoltaic and wind power conversion systems. Nevertheless, it is essential to implement innovative control strategies to enhance power quality in SMS, as the aforementioned authors have not included STSM controllers in their control approaches.

In order to achieve the best response of the proposed control method which designed by STSM controllers, various parameters must be obtain by using an optimization method under various operating conditions. Hence, HOA based algorithm is developed in this paper to estimate proper parameters of various STSM controllers. The detailed process involved in this estimation is given in next section.

3. HOA Based STSM Controller

Sliding mode control is a highly regarded control strategy that has received considerable acknowledgment in the context of various nonlinear systems [17,18]. The STSM controller is capable of resolving the chattering problems typically linked to conventional sliding mode control, thereby

 doi:10.20944/preprints202410.2581.v1

facilitating smooth control. The control law for this nonlinear system is articulated in the following way.

$$\begin{cases} u = a_2 |e|^{\frac{1}{2}} \operatorname{sgn}(e) + v \\ \dot{v} = a_3 \operatorname{sgn}(e) \end{cases} \quad (1)$$

Where, a_2 and a_3 are gains. e=a_1(input-reference)+differentiation of (input-reference).
Hence,

$$\text{Output} = a_2 \sqrt{e} \operatorname{sgn}(e) + \int a_3 \operatorname{sgn}(e) dt \quad (2)$$

Figure 2 illustrates the block diagram of the STSM control system. The adjustment of variables a_1, a_2, and a_3 presents significant challenges when employing multiple STSM controllers within the proposed control model. Consequently, the PSO method [17] is employed to estimate different parameters within the STSM controller. However, Hippopotamus Optimization Algorithm (HOA) has significance priority than PSO to identify the best solution [19]. In the process of developing the algorithm for the adaptive STSM controller, which involves the selection of design parameter values for the sliding mode control algorithm, a HOA approach was utilized and executed by equations (3) to (20).

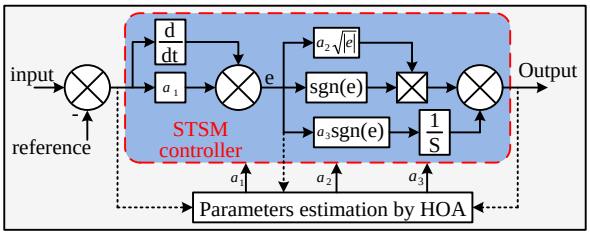

Figure 2. Symmetric diagram of STSM controller.

The function f(x) is influenced by the position of the STSM controller utilized in the proposed control methodology.

$$f = \int_0^T t.|input - reference|dt \quad (3)$$

The HOA algorithm is a population-based optimization method that represents basic mathematical equations using the following expressions.

$$H_i = B_j^L + k \times \left(B_j^U - B_j^L\right); i = 1,2,...N;\ j = 1,2,3...M \quad (4)$$

$$H = \begin{bmatrix} H_1 \\ \vdots \\ H_i \\ \vdots \\ H_N \end{bmatrix}_{N \times M} = \begin{bmatrix} h_{1,1} \cdots h_{1,j} \cdots h_{1,M} \\ \vdots \ \ddots \ \vdots \ \iddots \ \vdots \\ h_{i,1} \cdots h_{i,j} \cdots h_{i,M} \\ \vdots \ \ddots \ \vdots \ \iddots \ \vdots \\ h_{N,1} \cdots h_{N,j} \cdots h_{N,M} \end{bmatrix}_{N \times M} \quad (5)$$

The hippopotamus group has three behavioral procedures, as outlined previously, which are mathematically represented in the equations below.

Behavior -1: The current location of the hippos in the river or pond has been revised (Exploration): The leading hippopotamus is ascertained through the objective function value iteration. Normally, hippos have a tendency to congregate near each other. The dominant male hippos take on the role of protecting the herd and their territory from potential threats. Several female

 doi:10.20944/preprints202410.2581.v1

hippos are situated near the male hippos. The male hippopotamus members' positions within the lake or pond can be mathematically represented by the following equations.

$$H_i^{male} = h_{ij} + a_1 \bullet \left(D_h - a_2^{ij}\right) \tag{6}$$

$$b = \begin{cases} a_3 \times \vec{k}_1 + (\approx \delta_1) \\ 2 \times \vec{k}_2 - 1 \\ \vec{k}_3 \\ a_2 \times \vec{k}_4 + (\approx \delta_1) \\ \vec{k}_5 \end{cases} \tag{7}$$

$$H_i^{female} = \begin{cases} h_{ij} + b_1 \bullet \left(D_h - a_3^{ij} \bullet R_i\right) \exp\left(\frac{-t}{\tau}\right) > 0.6, else \\ h_{ij} + b_2 \bullet \left(R_i - D_h\right) k_6 > 0.5, else \\ B_j^L + k_7\left(B_j^U - B_j^L\right) \end{cases} \tag{8}$$

$$H_i = \begin{cases} H_i^{male} \times F_i^{male} < F_i; else \\ H_i \end{cases} \tag{9}$$

$$H_i = \begin{cases} H_i^{female} \times F_i^{female} < F_i; else \\ H_i \end{cases} \tag{10}$$

Behavior -2: Defence system of Hippopotamus against predators: The safety and security of hippopotamuses is a major contributing factor to their tendency to live in herds. Hippopotamuses primarily defend themselves by quickly turning towards the predator and emitting loud vocalizations to discourage the predator from getting too close. At this stage, Hippopotamuses may demonstrate a behavior of approaching the predator in order to make it retreat, effectively fending off the potential threat. Equations provided illustrate the location of the predator within the search space.

$$P_j = B_j^L + \vec{k}_8\left(B_j^U - B_j^U\right); \; j = 1,2.....M \tag{11}$$

$$\vec{G} = \left|P_j - H_{i,j}\right| \tag{12}$$

In this instance, the hippopotamus shifts its position towards the predator, albeit with a restricted range of motion. The aim is to alert the predator or intruder to its presence in its territory.

$$H_i^P = \begin{cases} \vec{R}_L \oplus P_j + \left(\frac{f}{\lambda \times \cos(2\pi j)}\right) \bullet \frac{F_{P_j}}{\vec{G}} < F_i \\ \vec{R}_L \oplus P_j + \left(\frac{f}{\lambda \times \cos(2\pi j)}\right) \bullet \frac{F_{P_j}}{2 \times \vec{G} + \vec{k}_9} \geq F_i \end{cases} \tag{13}$$

$$H_i = \begin{cases} H_i^{P_j} \times F_i^{P_j} < F_i \\ H_i \times F_i^{P_j} \geq F_i \end{cases} \tag{14}$$

The Levy distribution is employed to account for abrupt shifts in the predator's location when launching an attack on the hippopotamus. The mathematical formula for the stochastic motion of Levy movement is derived as follows.

 doi:10.20944/preprints202410.2581.v1

$$Levy(\eta) = \frac{0.05 \times \omega \times \left[\frac{\Gamma(1+\eta)\sin(\frac{\pi\eta}{2})}{\Gamma\left(\frac{1+\eta}{2}\right)\eta \times 2^{\frac{\eta-1}{2}}} \right]^{\frac{1}{\eta}}}{|\eta|^{\frac{1}{\eta}}} \quad (15)$$

Behavior -3: Escaping nature of Hippopotamus from the Predator: The hippopotamus exhibits a different behavior when faced with a predator, such as when it encounters a group of predators or is unable to fend off the predator using its defensive tactics. The approach results in the hippopotamus discovering a secure spot near its present whereabouts, and incorporating this conduct during third behavior of the HOA improves its capacity for local search exploitation.

$$_{local}B_j^L = \frac{B_j^L}{\gamma}; \quad _{local}B_j^U = \frac{B_j^U}{\gamma}; \gamma - 1,2,....\tau \quad (16)$$

$$H_i^{E_j} = H_{ij} + k_{10}\left(_{local}B_j^L + \psi\left(_{local}B_j^U - _{local}B_j^L\right)\right) \quad (17)$$

$$\psi = \begin{cases} 2 \times \vec{k}_{11} - 1 \\ k_{12} \\ k_{13} \end{cases} \quad (18)$$

$$H_i = \begin{cases} H_i^{E_j} \times F_i^{E_j} < F_i \\ H_i \times F_i^{E_j} \geq F_i \end{cases} \quad (19)$$

The best solution of above procedure from behavior 1 to 3 can be replaced as the best error signal (e) by below expression.

$$e_i = \begin{cases} H_i \times F_i, & < \xi; else; \\ H_i, \end{cases} \quad (20)$$

The procedure will continue to be executed until the optimal values of a_i are achieved. Respective flowchart of the proposed algorithm is shown in Figure 3.

 doi:10.20944/preprints202410.2581.v1

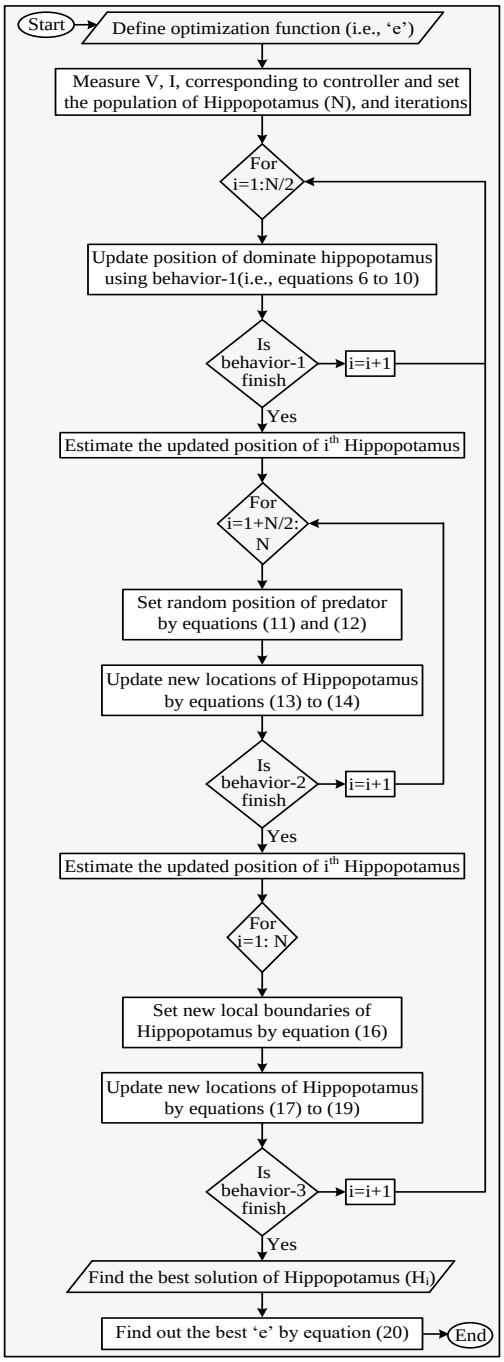

Figure 3. Flowchart of HOA for 'e'.

4. Mathematical Modeling of STSM Based Proposed System

Considered internal parameters of the Microgrid shown in Figure 1 as follows:
Internal resistance of wind MPPT (boost converter) =R_w.
Inductor of wind MPPT= L_w.
Duty cycle of MPPT = D_w.
Input voltage of MPPT = V_w.
Current flowing through MPPT = I_w.
Battery voltage = V_b.
Inductor of bidirectional converter = L_b.
Resistance of bidirectional converter = R_b.
Duty cycle of bidirectional converter = D_b.
Current flowing through bidirectional converter = I_b.

 doi:10.20944/preprints202410.2581.v1

Output voltage (i.e., dc-link voltage) =V_{dc}.

The generalized layout of wind-battery system with only their respective converters is shown in Figure 4.

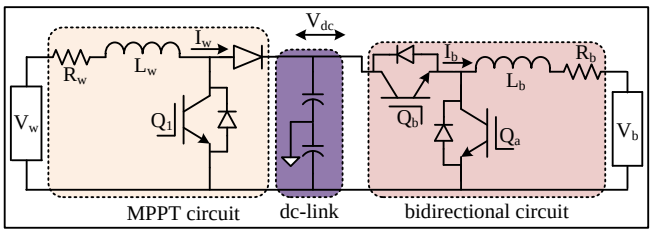

Figure 4. Generalized layout of wind, battery with their respective converters.

The following basic equations are obtained by using KVL law.

$$V_w = L_w \frac{dI_w}{dt} + R_w I_w + (1 - D_w) V_{dc} \tag{21}$$

$$V_b = L_b \frac{dI_b}{dt} + R_b I_b + (1 - D_b) V_{dc} \tag{22}$$

However, the battery current is in bidirectional flow and also duty cycle can be represented by

$$D_b = \begin{cases} 1 & if\ I_b > 0; \quad Q_b\ ON \\ 0 & if\ I_b < 0; \quad Q_a\ ON \end{cases} \tag{23}$$

In ideal case, input and output powers must be balanced, hence

$$P_w + P_{bat} = P_{load} \tag{24}$$

$$V_w I_{w,ref} + V_b I_{b,ref} = V_{dc} I_{dc,ref} \tag{25}$$

Hence,

$$I_{dc,ref} = \lambda \frac{(V_w I_{w,ref} + V_b I_{b,ref})}{V_{dc}} \tag{26}$$

Where, ' λ ' is the ideality factor which shows the power converters losses.

Considering errors of the system by {main errors signals of dc side controllers)

$$e_1 = I_w - I_{w,ref} \quad \{\text{which is used as STSM-1, refer Fig. 3}\} \tag{27}$$

$$e_2 = I_b - I_{b,ref} \quad \{\text{which is used as STSM-4, refer Fig. 4}\} \tag{28}$$

Similar analysis is also conducted for other STSM controllers.

The change in error is also considered,

$$\dot{e}_1 = \dot{I}_w - \dot{I}_{w,ref} \tag{29}$$

$$\dot{e}_2 = \dot{I}_b - \dot{I}_{b,ref} \tag{30}$$

Therefore,

$$\dot{e}_1 = \frac{V_w}{L_w} - \frac{R_w}{L_w} I_w - \frac{(1 - D_w)}{L_w} V_{dc} - \dot{I}_{w,ref} \tag{31}$$

Preprints.org (www.preprints.org) | NOT PEER-REVIEWED | Posted: 31 October 2024 doi:10.20944/preprints202410.2581.v1

$$\dot{e}_2 = \frac{V_b}{L_b} - \frac{R_b}{L_b} I_b - \frac{(1-D_b)}{L_b} V_{dc} - \dot{I}_{b,ref} \tag{32}$$

Similar approach is also conducted for other STSM controllers based on their error signals.

5. Proposed Control Methodologies

1. MPPT control of WPCS [3]:

The wind turbine's speed signal, essential for the effective execution of MPPT in WPCS, is frequently difficult to acquire and susceptible to errors in current methodologies. Therefore, a P&O method is employed that necessitates only voltage and current signals, which are derived from the dc-link and the current injected into the dc-link from the WPSC (i.e., I_w), as illustrated in Figure 1. To minimize the number of sensors required, the approach is executed by focusing on the voltage at the dc-link (i.e., V_{dc}) rather than the voltage across the three-phase diode rectifier. The application of the P&O algorithm enables the system to follow the reference current, which varies with wind speed, to optimize power generation. The P&O approach for WPCS is derived from the fundamental equation presented below.

$$I_w^{k+1} = I_w^k + \Delta I_w \times sign\left(\frac{dP_w}{dI_w}\right) \tag{33}$$

The output signal generated by the P&O algorithm is subsequently compared with the actual wind current (i.e., I_w). The STSM controller-1 will receive the error signal to produce the necessary pulses for switch Q_1, which is utilized in the MPPT circuit of the WPCS. Figure 5 presents a diagrammatic representation of the proposed control strategy for the MPPT of WPCS.

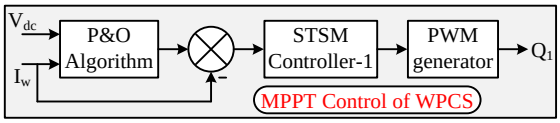

Figure 5. Proposed MPPT control of WPCS.

2. Control of bidirectional circuit:

The oversight of the charging and discharging operations of the BSU is significantly dependent on the regulation of the bidirectional DC to DC converter. This converter is essential for managing the energy transfer between the battery bank and the external power source or load. The bidirectional DC to DC circuit regulates the current flow from the WPCS to the BSU throughout the charging process. It guarantees that the charging current remains within safe parameters, thereby preventing overcharging and possible harm to the batteries by taking the SoC into account. Conversely, throughout the discharging process, the bidirectional DC to DC circuit regulates the current flow from the BSU to the load. It guarantees that the discharging current is supplied at the necessary voltage and current specifications, thereby offering a consistent power supply to the load. The converter additionally oversees the battery voltage and modifies the discharging current to avert excessive discharge, which may result in diminished battery lifespan.

The regulation of the bidirectional DC to DC circuit is generally accomplished using an advanced control algorithm illustrated in Figure 6. The fluctuating aspect of the dc-link voltage is also eliminated to enhance the fatigue lifespan of the wind turbine shaft. In addition, the control algorithm integrates multiple protective measures to guarantee the safety and dependability of the BSU. This converter is essential for managing energy flow, enhancing the efficiency of both charging and discharging processes, and guaranteeing the safety and dependability of the BSU.

Preprints.org (www.preprints.org) | NOT PEER-REVIEWED | Posted: 31 October 2024 doi:10.20944/preprints202410.2581.v1

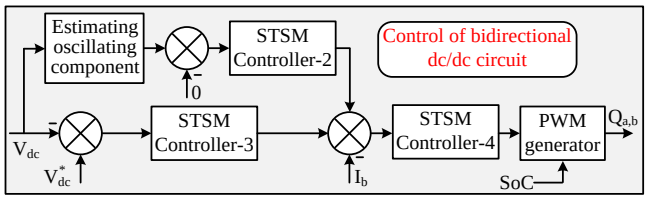

Figure 6. Control method of the bidirectional dc/dc circuit.

3. Control of inverter:

The inverter's control strategy entails overseeing the frequency and voltage levels at the PLB, while implementing real-time modifications to the inverter output to guarantee that these parameters stay within permissible limits. The proposed inverter control strategy enhances system stability and reliability by efficiently regulating frequency and voltage levels, thereby optimizing both the performance of the inverter and the overall SMS. This control strategy holds significant importance in renewable energy systems, as variations in generation can affect the frequency and voltage levels at the load bus. The adoption of the inverter control proposal enables operators to maintain efficient and reliable operation of the power system, even amidst fluctuating generation patterns. Variations in load at PLB can lead to fluctuations in frequency; therefore, the reference current of the dc-bus (i^*_{dc}) is generated by the STSM controller-5 through a comparison of the frequency with its designated reference value. In a similar manner, the generation of reference quadrature current facilitates the provision of reactive power, which is necessitated by the reactive power demands of loads at PLB. The control method proposed is illustrated in Figure 7.

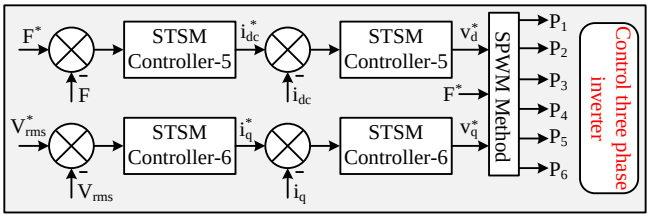

Figure 7. Proposed control of the inverter.

6. Small Signal Analysis of Proposed Method

The mathematical transfer function of the Microgrid model has been developed to analyze the effectiveness of the proposed control method in regulating voltage during transient response scenarios. The development of the suggested mathematical model for the Wind-battery Microgrid through the Transfer Function presents difficulties owing to the presence of nonlinear elements within the Microgrid, including the PMSG-wind turbine, BSU, converters, and inverter systems [20,21]. Typically, the Microgrid operates as a multi-input, multi-output system characterized by two control loops: the outer voltage control loop and the inner current control loop. Generalized transfer functions of the wind and BSU are expressed by following equations.

$$G_{WS} = \frac{K_{WS}}{sT_{WS}+1} \quad \text{and} \quad G_{BSU} = \frac{K_{BSU}}{sT_{BSU}+1} \tag{34}$$

Where, K_{WS} and K_{BSU} are first order lagging systems of gains and time constants represents T_{WS} and T_{BSU} for wind and BSU respectively.

Similarly transfer functions of converters are:

$$G_{MPPT} = \frac{K_{MPPT}}{sT_{MPPT}+1} \tag{35}$$

$$G_{inv} = \frac{K_{inv}}{sT_{inv}+1} \tag{36}$$

Preprints.org (www.preprints.org) | NOT PEER-REVIEWED | Posted: 31 October 2024 doi:10.20944/preprints202410.2581.v1

Regarding the bidirectional circuit of the battery, there are two modes, and respective state space equations can be represented by:

Current controller for boost mode:

$$\frac{d}{dt}[\tilde{x}_{c1}] = [0][\tilde{x}_{c1}] + [-1][\tilde{i}_b] \tag{37}$$

$$[\tilde{d}_{c1}] = [STSM][\tilde{x}_{c1}] + [-STSM][\tilde{i}_b] \tag{38}$$

Current controller for boost mode:

$$\frac{d}{dt}[\tilde{x}_{c2}] = [0][\tilde{x}_{c2}] + [-1][\tilde{i}_b] \tag{39}$$

$$[\tilde{d}_{c2}] = [-STSM][\tilde{x}_{c2}] + [STSM][\tilde{i}_b] \tag{40}$$

The layout of the proposed system with respective transfer functions is shown in Figure 8. The transfer function for dc side is expressed by:

$$\frac{\Delta V_{dc}}{\Delta V_{dc}^*} = \frac{(n_2 s^3 + n_3 s^2 + n_4 s) + n_1}{(f_1)s^4 + (f_2)s^3 + (f_3)s^2 + (f_4)s + f_5} \tag{41}$$

Where $n_{1\text{-}4}$ are constants and $f_{1\text{-}5}$ are functions with respective STSM controller parameters.

$$f_1 = F(L, C); \tag{42}$$

$$f_{2,3} = F(R, C, L, a_2 |e|^{\frac{1}{2}} \operatorname{sgn}(e)); \tag{43}$$

$$f_3 = F(R, C, L, a_2 |e|^{\frac{1}{2}} \operatorname{sgn}(e), a_3 \operatorname{sgn}(e)); \tag{44}$$

$$f_4 = F(R, C, L, a_3 \operatorname{sgn}(e)); \tag{45}$$

$$f_5 = F(R, C, L, v); \tag{46}$$

The parameters involved in above functions are obtained by using HOA method.

Figure 8 can be further modified by representing simple voltage and current loops. The inner loop is current and outer loop is voltage control. For understanding purpose, the Figure 8 up to DC side is represented by simple control loops as depicted in Figure 9.

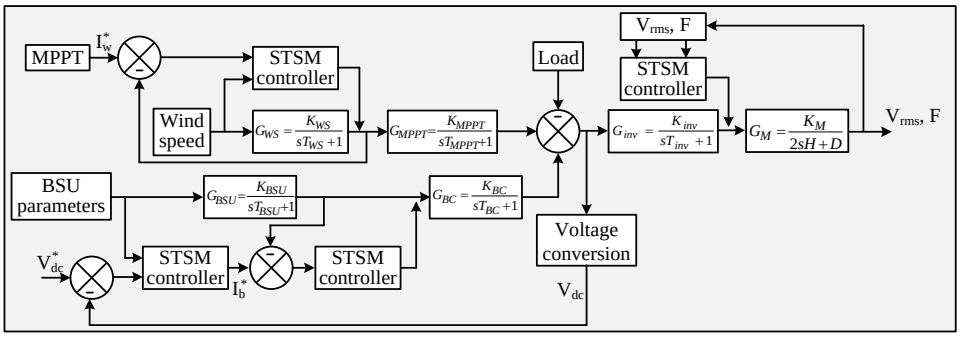

Figure 8. Small signal schematic block diagram of SMS.

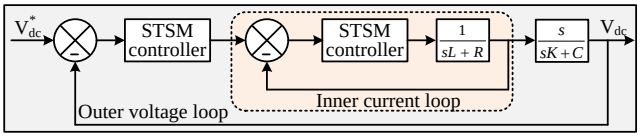

 doi:10.20944/preprints202410.2581.v1

Figure 9. Control loops of the SMS.

7. Results Through HIL

The OPAL-RT platform serves as an advanced instrument for performing HIL testing [22–25] on SMSs. Performing HIL tests on the OPAL-RT platform offers an in-depth insight into the various results that may emerge in a SMS. These assessments enable researchers and engineers to replicate a range of scenarios and analyze the various results that may emerge in a SMS. A potential result that can be demonstrated through HIL testing is the effective incorporation of renewable energy sources into the SMS. Researchers can analyze the system's response to the variable power output from wind turbines by simulating their integration with the SMS. An additional result that can be examined through HIL testing is the reaction of the SMS to abrupt fluctuations in load demand. Through the simulation of scenarios characterized by rapid fluctuations in load demand, researchers are able to analyze the adjustments made by the SMS in its power generation and distribution processes to accommodate the altered demand. This may assist in recognizing any possible challenges or constraints within the system, thereby facilitating necessary enhancements.

The setup for HIL is executed utilizing two OPAL-RT units [19,24]. The first OPAL-RT unit accommodates a plant that includes WPCS, BSU, converters, LC components, and AC loads, while the proposed control strategy illustrated in Figures 3–5 is implemented in the second OPAL-RT unit. These two units are linked to input/output devices to facilitate potential data transfer. Different waveforms can be detected in an alternative system. The comprehensive block diagram illustrating the establishment of HIL is presented in Figure 10. The detailed implementation of HIL block of the proposed method with color coding is depicted in Figure 11 for more clarity. Various sensors are used to obtain signals of currents, voltages and SoC of the battery from the plant to send control unit which are denoted by green color. These signals are converted into digital forms and sent as input signals into control unit. The control unit will produce required digital signals for various converters used in plant. These signals further converted into analogue and sent to plant unit, which are denoted by red color. This section presents a variety of results utilizing HIL as follows.

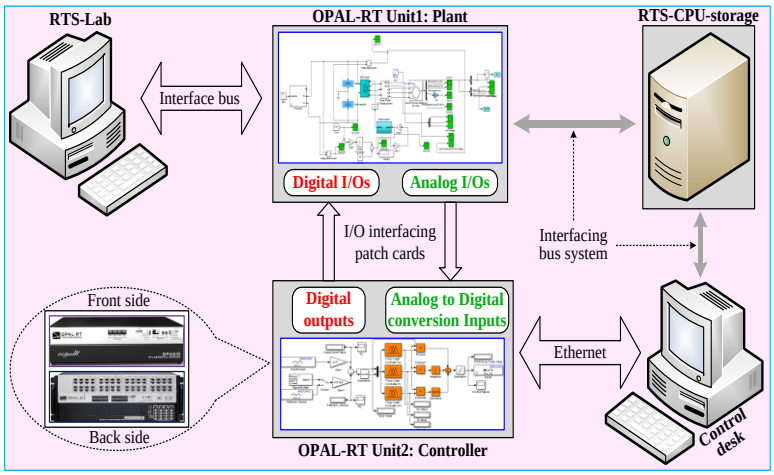

Figure 10. Establishment of HIL.

 doi:10.20944/preprints202410.2581.v1

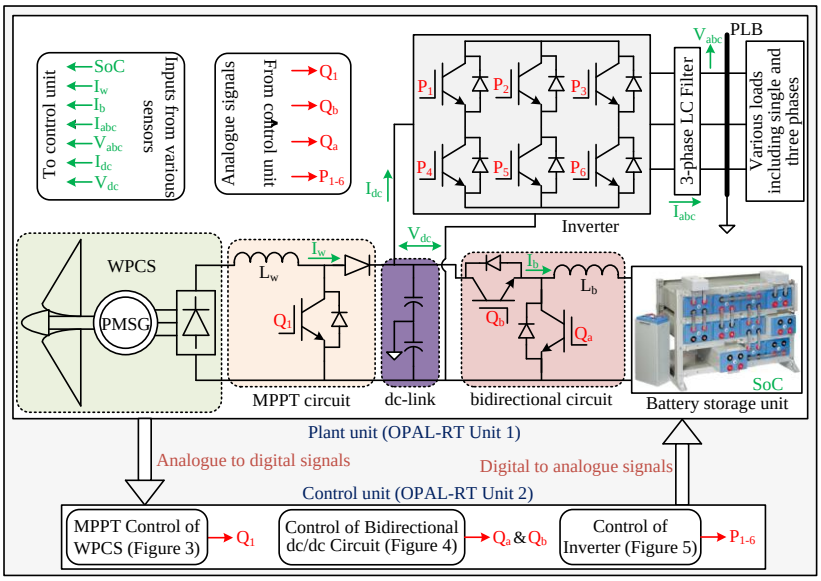

Figure 11. Detailed HIL configuration of the proposed system.

Test-1: Comparison of STSM with various controllers:

The SMS undergoes testing at a load variation of 200% at PLB, utilizing STSM, Fuzzy, and PI controllers. The load is introduced at 1.5 seconds and removed at 1.65 seconds. Throughout this time frame, an analysis of the frequency response among STSM, Fuzzy, and PI controllers is conducted and illustrated in Figure 12. The frequency response achieved with the STSM controllers is stable and reaches equilibrium rapidly. Consequently, additional tests are performed utilizing the proposed control strategy with STSM controllers.

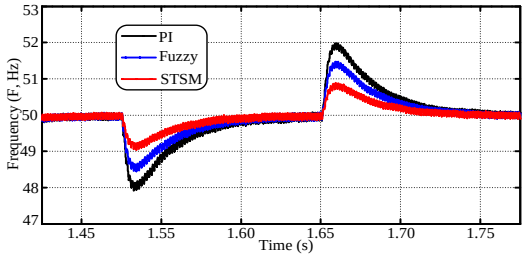

Figure 12. Response of frequency with STSM, Fuzzy and PI controller.

Test-2: Response under load change:

A complete change in load is observed at t=1.5 seconds, with the release occurring at t=2 seconds. Throughout this timeframe, the suggested control methodology effectively stabilized the voltages at both the dc-link and PLB. The voltage at the DC link is illustrated in Figure 13, while the corresponding response of the three-phase voltages at PLB is presented in Figure 14. The stable voltage at dc-link is observed in Figure 13 which indicates the effectiveness of developed EMS by proposed control methodology. Balanced and stabilized RMS voltages are supplied at PLB (as per Figure 14) which represents the good power quality by proposed method. Therefore, the proposed methodology helps to maintain both EMS as well as improving power quality.

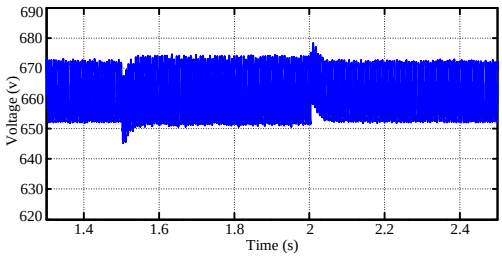

 doi:10.20944/preprints202410.2581.v1

Figure 13. Response of voltage at dc-link.

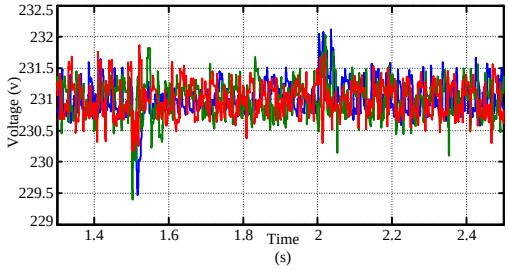

Figure 14. Three phase voltages at PLB.

Test-3: Response under change in wind speed:

The SMS response is evaluated in relation to variations in wind speed. The wind speed is altered at t = 2.0 seconds, while the load is simultaneously increased at t = 1.75 seconds. In the event of a variation in wind speed, the suggested control methodology for MPPT effectively monitors the maximum power, as illustrated in Figure 15, which also presents the response of torques. Therefore the proposed control of MPPT is depicted in Figure 5 is working effectively under rapid change in the speed of the wind. The respective powers of the load, BSU, and WPCS are illustrated in Figure 16. From Figure 16, it is observed that the EMS is helps to BSU to respond according to power balance between generation and the load at PLB.

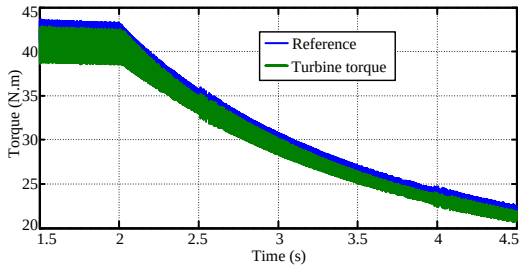

Figure 15. Response of torque of WPCS.

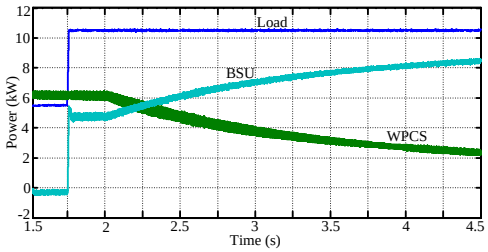

Figure 16. Various powers in SMS.

Test-4: Performance of HOA.

The response of the error signal from V_{rms} is considered for comparison among proposed HOA, PSO, STSM (simple tuned STSM control) and Conventional PI controller. A step change of 75% load is applied at t=7.50 seconds at PLB for testing in this case. Various parameters of STSM controllers used in the proposed method are obtained from HOA, PSO, and ITSE method. Utilizing these parameters, the error signal response (expressed as a percentage of the normalized value derived from the equation below) is illustrated in Figure 17. By observing Figure 17, the response has improved by using proposed method with HOA. Error is very nominal in the case of optimized parameters by using HOA.

 doi:10.20944/preprints202410.2581.v1

$$\%\ \text{of nornalized}\, V_{rms} = \frac{V_{rms}^{*} - V_{rms}}{V_{rms}^{*}} \times 100 \tag{47}$$

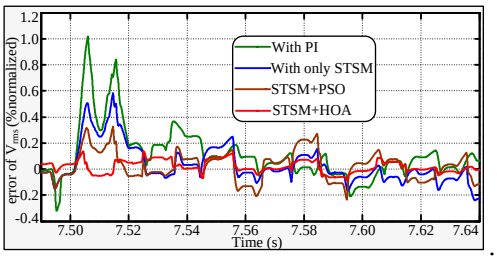

Figure 17. Response of error signal.

Test-5: Convergence with HOA.

Various parameters of STSM controller is obtained by using Grey Wolf Optimization (GWO), Whale Optimization Algorithm (WOA) and HOA. The convergence of the respective algorithms is depicted in Figure 18 and found that the HOA having best response as compared with others. This implies, the response of controller is improved by the proposed STSM-HOA method.

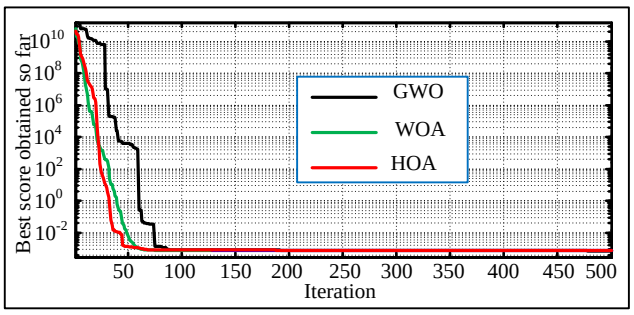

Figure 18. Convergence of HOA over GWO and WOA.

Test-6: Responses with small signal analysis.

The Bode plot, which illustrates the gain and phase margins for the loop transfer function (41) of SMS, is displayed in Figures 19. These show that the system is well robust. This signifies that the inner loop is much faster than the outer loop. The phase margin is observed at 96^0 which is high robust due to the proposed control method based on STSM controllers.

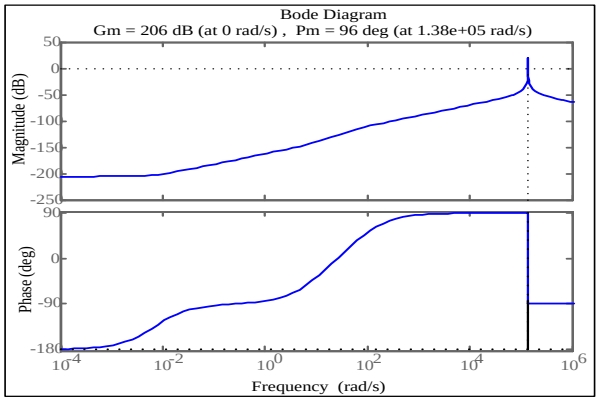

Figure 19. Frequency response for phase and gain margins.

In the similar way, response for small changes in reference of the V_{dc} is also carried out. Small changes for decreasing and increasing of change in V_{dc} are applied at t=3.0 and 4.0 sec. Corresponding

 doi:10.20944/preprints202410.2581.v1

response for actual dc-link voltage is depicted in Figure 20. By observing Figure 20, a stable response is observed and the actual dc-link voltage is faster enough to follow its reference value.

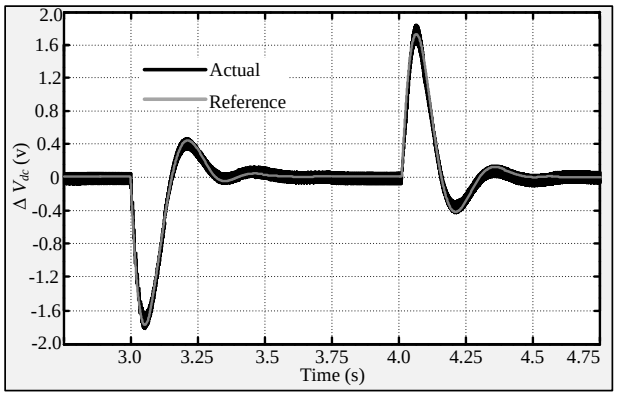

Figure 20. Response of change in dc-link voltage.

8. Conclusion

This paper introduces a new control strategy aimed at enhancing the power quality of WPCS-BSU based SMS, utilizing STSM controllers for its implementation. The suggested control methodology is additionally evaluated against Fuzzy and PI controllers. The HOA method is used to adjust various parameters of the STSM controllers. The proposed methodology holds considerable precedence over alternative methods. An EMS was also established alongside various components integrated within the SMS. A range of outcomes is presented and examined through HIL testing on the OPAL-RT platform. Listed results are satisfactory to improve the power quality under various operating conditions. Detailed analysis for robustness of the system is also incorporated in this paper with the help of small signal analysis. From various findings, observed that, the proposed system is stabled under various changes in the system.

Nomenclature:

WPCS: Wind Power Conversion System.
PMSG: Permanent Magnet Synchronous Generator.
SMS: Standalone Microgrid System.
STSM: Super Twisting Sliding Mode.
BSU: Battery Storage Unit.
HIL: Hardware – in the – Loop.
MPPT: Maximum Power Point Tracking.
EMS: Energy Management System.
HOA: Hippopotamus Optimization Algorithm
PLB: Point of Load Bus.

References

1. H. Zhang, Y. Chen, Y. Gao, M. Zhao, H. Wang and Z. Lei, "Research on Energy Conversion Benefits of Hybrid Wind Power and Concentrating Solar Power System Based on Time-of-use Electricity Price," 2023 24th International Conference on Electronic Packaging Technology (ICEPT), Shihezi City, China, 2023, pp. 1-5, doi: 10.1109/ICEPT59018.2023.10492026.
2. R. Akbari and A. Izadian, "Reduced-Size Converter in DFIG-Based Wind Energy Conversion System," 2020 IEEE Energy Conversion Congress and Exposition (ECCE), Detroit, MI, USA, 2020, pp. 4217-4223, doi: 10.1109/ECCE44975.2020.9236110.
3. A. S. Badawi, N. F. Hasbullah, S. H. Yusoff, A. Hashim, S. Khan and A. M. Zyoud, "Paper review: maximum power point tracking for wind energy conversion system," 2020 2nd International Conference on Electrical, Control and Instrumentation Engineering (ICECIE), Kuala Lumpur, Malaysia, 2020, pp. 1-6, doi: 10.1109/ICECIE50279.2020.9309567.

4. Q. Gao, N. Ertugrul, B. Ding and M. Negnevitsky, "Offshore Wind, Wave and Integrated Energy Conversion Systems: A Review and Future," 2020 Australasian Universities Power Engineering Conference (AUPEC), Hobart, Australia, 2020, pp. 1-6.
5. W. Chen, W. Yang, Q. Chen, J. Li and H. Geng, "Wind Speed Estimation for PMSG-Based WECS under Power Limit Control," 2023 IEEE 6th International Electrical and Energy Conference (CIEEC), Hefei, China, 2023, pp. 1288-1292, doi: 10.1109/CIEEC58067.2023.10166912.
6. Â. M. M. dos Santos, R. P. C. Pacífico, N. S. Costa, M. V. S. de França, V. S. de C. Teixeira and A. B. Moreira, "Control of SCIG Based on Wind Energy Conversion System with BESS," 2023 IEEE 8th Southern Power Electronics Conference and 17th Brazilian Power Electronics Conference (SPEC/COBEP), Florianopolis, Brazil, 2023, pp. 1-7, doi: 10.1109/SPEC56436.2023.10407111.
7. Malla, Priyanka, Malla, Siva Ganesh and Calay, Rajnish Kaur. "Voltage control of standalone photovoltaic – electrolyzer- fuel cell-battery energy system" *International Journal of Emerging Electric Power Systems*, vol. 24, no. 5, 2023, pp. 649-658. https://doi.org/10.1515/ijeeps-2022-0047.
8. Vankudothu Balu, K Krishnaveni, Priyanka Malla and Siva Ganesh Malla, "Improving the power quality and hydrogen production from renewable energy sources based microgrid", IOP: Engineering Research Express, Volume 5, Number 3, August 2023, DOI 10.1088/2631-8695/acecdb.
9. S. S. Prasad, K. Deepak, D. Vannurappa, Y. S. I. Priyadarshini, M. B. Lakshmi and S. G. Malla, "Novel Control Scheme for Wind based Standalone Hybrid Power Generation System under Faults on Three Phase Distribution Feeders," 2023 7th International Conference on Computing Methodologies and Communication (ICCMC), Erode, India, 2023, pp. 21-26, doi: 10.1109/ICCMC56507.2023.10084134.
10. Y. I. P. Darshini, K. Deepak, U. Chaithanya, Y. Hazarathaiah, D. Vannurappa and D. S. G. Malla, "Power Quality Improvement of Standalone Microgrid during Faults on Distribution Line with DSTATCOM," 2023 5th International Conference on Smart Systems and Inventive Technology (ICSSIT), Tirunelveli, India, 2023, pp. 530-536, doi: 10.1109/ICSSIT55814.2023.10061071.
11. U. T. Salman, F. S. Al-Ismail and M. Khalid, "Optimal Sizing of Battery Energy Storage for Grid-Connected and Isolated Wind-Penetrated Microgrid," in IEEE Access, vol. 8, pp. 91129-91138, 2020, doi: 10.1109/ACCESS.2020.2992654.
12. S. Puchalapalli, B. Singh and S. Das, "Grid-Interactive Smooth Transition Control of Wind-Solar-DG Based Microgrid at Unpredictable Weather Conditions," in IEEE Transactions on Industry Applications, vol. 60, no. 1, pp. 1519-1529, Jan.-Feb. 2024, doi: 10.1109/TIA.2023.3322396.
13. Malla, Siva Ganesh, Malla, Jagan Mohana Rao, Malla, Priyanka, Ramasamy, Sreekanth, Doniparthi, Satish Kumar, Sahu, Manoj Kumar, Subudhi, Pravat Kumar and Awad, Hilmy. "Coordinated power management and control of renewable energy sources based smart grid" *International Journal of Emerging Electric Power Systems*, vol. 23, no. 2, 2022, pp. 261-276. https://doi.org/10.1515/ijeeps-2021-0113
14. E. Dehghanpour, H. K. Karegar and R. Kheirollahi, "Under Frequency Load Shedding in Inverter Based Microgrids by Using Droop Characteristic," in IEEE Transactions on Power Delivery, vol. 36, no. 2, pp. 1097-1106, April 2021, doi: 10.1109/TPWRD.2020.3002238.
15. T. Anuradha et al., "Power Quality Improvement of Hybrid Standalone Microgrid with DSTATCOM during Faults on Distribution Line," 2022 IEEE International Conference on Power Electronics, Drives and Energy Systems (PEDES), Jaipur, India, 2022, pp. 1-7, doi: 10.1109/PEDES56012.2022.10080027.
16. S. G. Malla, P. K. Dadi and J. Dadi, "Wind and photovoltaic based hybrid stand-alone power generation system," 2017 International Conference on Energy, Communication, Data Analytics and Soft Computing (ICECDS), Chennai, India, 2017, pp. 3718-3725, doi: 10.1109/ICECDS.2017.8390158.
17. M. Dai, R. Qi and X. Cheng, "Super-Twisting Sliding Mode Control Design for Electric Dynamic Load Simulator," 2019 Chinese Control Conference (CCC), Guangzhou, China, 2019, pp. 3078-3083, doi: 10.23919/ChiCC.2019.8865725.
18. A. Del Pizzo, L. P. Di Noia and S. Meo, "Super twisting sliding mode control of smart-inverters grid-connected for PV applications," 2017 IEEE 6th International Conference on Renewable Energy Research and Applications (ICRERA), San Diego, CA, USA, 2017, pp. 793-796, doi: 10.1109/ICRERA.2017.8191168.
19. Amiri, M.H., Mehrabi Hashjin, N., Montazeri, M. et al. Hippopotamus optimization algorithm: a novel nature-inspired optimization algorithm. Sci Rep 14, 5032 (2024). https://doi.org/10.1038/s41598-024-54910-3.
20. D. Kumar, H. D Mathur, S. Bhanot, R.C. Bansal, Modeling and frequency control of community microgrids under stochastic solar and wind sources, Engineering Science and Technology, an Int. Journal 23 (2020) 1084–1099. Elsevier.
21. Y.V.P. Kumar, R. Bhimasingu, Design of Voltage and Current Controller Parameters Using Small Signal Model-Based Pole-Zero Cancellation Method for Improved Transient Response in Microgrids, SN Applied Sciences, 2021.
22. V M Revathi et al, "A modified invasive weed optimization for MPPT of PV based water pumping system driven by induction motor, IOP: Engineering Research Express, volume 6, number 3, July 2024, 10.1088/2631-8695/ad5cd3.

23. X. Fu, A. Javadi, K. Al-Haddad, L. -A. Dessaint, W. Li and B. -T. Ooi, "HIL-RT Implementation of UHVDC Transmission System Based on Series-Connected VSC Modules," in IEEE Access, vol. 7, pp. 84602-84612, 2019, doi: 10.1109/ACCESS.2019.2925032.
24. C. Sun et al., "Design and Real-Time Implementation of a Centralized Microgrid Control System With Rule-Based Dispatch and Seamless Transition Function," in IEEE Transactions on Industry Applications, vol. 56, no. 3, pp. 3168-3177, May-June 2020, doi: 10.1109/TIA.2020.2979790.
25. C. Sun et al., "Design and Real-Time Implementation of a Centralized Microgrid Control System With Rule-Based Dispatch and Seamless Transition Function," in IEEE Transactions on Industry Applications, vol. 56, no. 3, pp. 3168-3177, May-June 2020, doi: 10.1109/TIA.2020.2979790.